PCCP

RSC Publishing

PAPER

View Article Online
View Journal | View Issue

Analytical theory and stability analysis of an elongated nanoscale object under external torque†

Cite this: *Phys. Chem. Chem. Phys.*, 2013, **15**, 10817

Arijit Ghosh,[a] Pranay Mandal,*[b] Suman Karmakar[b] and Ambarish Ghosh‡*[b]

Received 15th February 2013,
Accepted 30th April 2013

DOI: 10.1039/c3cp50701g

www.rsc.org/pccp

We consider the rotational motion of an elongated nanoscale object in a fluid under an external torque. The experimentally observed dynamics could be understood from analytical solutions of the Stokes equation, with explicit formulae derived for the dynamical states as a function of the object dimensions and the parameters defining the external torque. Under certain conditions, multiple analytical solutions to the Stokes equations exist, which have been investigated through numerical analysis of their stability against small perturbations and their sensitivity towards initial conditions. These experimental results and analytical formulae are general enough to be applicable to the rotational motion of any isolated elongated object at low Reynolds numbers, and could be useful in the design of non-spherical nanostructures for diverse applications pertaining to microfluidics and nanoscale propulsion technologies.

I Introduction

Recent advances in nanotechnology have led to the integration[1] of synthesis and actuation technologies of multifunctional nanoparticles for novel applications aimed towards sensing, microrheological measurements, mixing and delivery of chemicals, to name a few. A large section of these objects are non-spherical, and quite often rod-shaped, which have been actuated by externally applied electric,[2] magnetic[3–5] or optical[6–8] forces. Such systems have been used for precise nanomanipulation for a variety of applications, such as local rheological[9,10] probes of the surrounding environment, synthesis of nanocomposites[11] and ferrogels,[12] mixing fluids[13] and manipulating "dust"[2] in microfluidic devices *etc.* A recent area of application with growing interest[14–16] is in the actuation of non-spherical nanoscale objects through the coupling of a permanent (or induced) magnetic, or electric dipole moment with an external torque applied through rotating magnetic, or electric fields, such as to couple the rotational motion around one of the body axes to translational motion along another degree of freedom, where the coupling could arise either due to intrinsic chirality[17,18] in the object shape, or through the presence of a surface.[19] Understanding how the dynamics of externally actuated non-spherical objects depend on the geometrical characteristics of the object, and the parameters defining the external torque, *e.g.* frequency and magnitude of the external rotating fields, will be important in designing and actuating nanostructures with enhanced functionalities.

At nanoscale dimensions, motion is typically dominated by viscosity (low Reynolds number), under which condition there is no variational principle[20] that can predict the motion in a general manner. For simple geometries and systems, such as spherical nanostructures with a permanent moment (electric or magnetic) under a torque of magnitude τ arising due to coupling with an externally applied field (electric or magnetic) rotating at frequency Ω, analytical solutions predict the rigid body dynamics accurately.[21] It can be easily shown that the moment and therefore the sphere, rotates at the same angular speed as that of the field until a critical frequency Ω_c, after which the rotational viscous drag can not be overcome by the applied torque. This results in a phase slip motion of the sphere with an average angular velocity $\Omega_{slip} = \Omega - \sqrt{\Omega^2 - \Omega_c^2}$, where Ω_c is the ratio between the applied torque and the viscous drag coefficient γ_r, which in turn is related to the radius r of the sphere, and viscosity η of the surrounding medium, given by $\gamma_r = 8\pi\eta r^3$. The simplicity of this problem is essentially due to the presence of one degree of rotational freedom present in a sphere, while an elongated object such as a rod, has multiple degrees of freedom giving rise to a set of coupled

[a] *Department of Electrical Communication Engineering, Indian Institute of Science, Bangalore 560012, India*
[b] *Centre for Nano Science and Engineering, Indian Institute of Science, Bangalore 560012, India. E-mail: pranaymandal13@cense.iisc.ernet.in, ambarish@ece.iisc.ernet.in*

† Electronic supplementary information (ESI) available. See DOI: 10.1039/c3cp50701g

‡ Also at Department of Physics, Department of Electrical Communication Engineering, Indian Institute of Science, Bangalore 560012, India.

differential equations. The relevant drag coefficients for a rod like object are related to rotation around the long and short axes,[22] given by $\gamma_l = \frac{\pi\eta}{0.96}\frac{a^3(1+C_r^{\parallel})}{p^2}$ and $\gamma_s = \frac{\pi\eta}{3}\frac{a^3}{\ln(p)+C_r^{\perp}}$ respectively, where a is the length of the rod, p is the length to diameter ratio of the rod, $C_r^{\parallel} = \frac{0.677}{p} - \frac{0.183}{p^2}$ and $C_r^{\perp} = -0.662 + \frac{0.917}{p} - \frac{0.05}{p^2}$. Analytical solutions to these equations have been previously obtained under special conditions,[23] for example in rods with permanent moments along their long axis, or in cases where the motion of the rod has been confined in two dimensions. In the most general case, the moment can be along an arbitrary direction with respect to the body frame of the elongated object, in which case the experimentally observed dynamics show two distinct regimes of rotational motion around the long and the short axes, which have also been confirmed through numerical[24,25] calculations. In this paper, we have derived analytical solutions to the three dimensional problem of rotation of a small rod-like object under external torque in a low Reynolds number environment, and provided explicit formulae for the conditions at which transitions between various dynamical regimes occur. While the analytical and experimental results match very well, under certain conditions multiple solutions to the equations exist, whose stabilities against small perturbations have been investigated using numerical methods. The analysis presented here is valid for any elongated object that can be described with two distinct rotational drag coefficients, thereby including a wide variety of shapes including rods, ellipsoids, helices, discs *etc*.

II Experimental observations

The experimental system discussed here was a helical nanostructure with a permanent magnetic moment of magnitude m that made an angle θ_m with the short axis of the object. When dispersed in a fluidic medium, such as deionized water and subjected to a rotating magnetic field of magnitude B and rotation frequency Ω_B, the helical nanostructures were observed to demonstrate various dynamical configurations. The details of the experimental setup can be found elsewhere (ref. 18 and 24 and the corresponding ESI†). Ref. 24 includes movies and descriptions pertaining to the various dynamical configurations. The most important observable was the orientation of the object, given by the precession angle θ that the long axis of the rotating helical nanostructure made with the normal to the plane of rotation of the magnetic field. It may be noted that the experimental quantity $\tilde{\theta}$ is the 2D projection of the actual precession angle as observed in an optical microscope. Under such circumstances the average value of θ is measured as $\theta_{avg} = \sqrt{2}\sigma_{\tilde{\theta}}$, where $\sigma_{\tilde{\theta}}$ is the standard deviation of $\tilde{\theta}$. In Fig. 1, $\cos\theta_{avg}$ as a function of magnetic field rotation frequency, Ω_B, is plotted, for a helix having a magnetization angle $\theta_m \approx 18^\circ$ and a magnetic field $B = 60$ G. At low frequencies, the object "tumbled" with $\theta = 90^\circ$ *i.e.* it rotated about its short axis (see schematic), in the plane of rotation of the magnetic field. As the frequency was increased beyond a particular frequency Ω_1^{expt} (6 Hz in this case), the helix came out of the plane and started to "precess" (see schematic) at a steady value of θ. The precession angle decreased with increase in magnetic field frequency up to a step out frequency Ω_2^{expt} (130 Hz in this case), after which the precession angle did not have a steady state constant value, but rather fluctuated randomly between tumbling and precessional configurations. Fig. 1 also shows (black solid line) a theoretical curve for $\cos\theta$ where $\theta = \sin^{-1}(\Omega_1/\Omega_B)$, where theoretical expressions for θ, $\Omega_1 = \Omega_1^{expt}$, as well as $\Omega_2 = \Omega_2^{expt}$ are derived in Section III. These quantities depend on the two rotational drag coefficients of the elongated object, the magnitude of the torque and the moment angle θ_m. The estimates of these quantities as applicable to the experimental system have are in the ESI,† S1. The stabilities of the different dynamical states are discussed in Section IV.

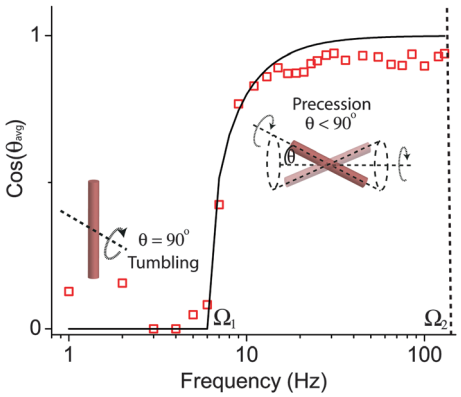

Fig. 1 Experimentally obtained values (red squares) of $\cos\theta_{avg}$ as a function of the magnetic field frequency Ω_B. Black (solid) line shows the corresponding theoretical curve, discussed in Section III.

III Theory

We follow Euler's x convention, where three angles, namely ϕ, θ and ψ, are used to describe the generalized orientation of a rod-like object, as shown in Fig. 2(A). The object with its long axis along the body fixed z' axis, is subjected to a magnetic field of strength B, rotating in the lab fixed xy plane with frequency Ω_B. The magnetic moment $\vec{m}$ of the ellipsoid is supposed to be in the body $x'z'$ plane making an angle θ_m with its short axis (x' axis). The rotating magnetic field exerts a magnetic torque $\vec{\tau}$ on the object. If γ is the rotational friction tensor and $\vec{\omega}$ is the angular velocity vector, the time evolution of the dynamics is given by,

$$\vec{\tau} = \gamma\vec{\omega}, \qquad (1)$$

where $\vec{\tau} = \vec{m} \times \vec{B}$. Typical nanostructure dynamics in microfluidic environments imply a low Reynolds number ($Re \ll 1$), and therefore it is justified to neglect inertial terms in writing eqn (1). The equation is solved in the body frame ($x'y'z'$) of the object, whose rotational friction coefficients about its long and short axis are γ_l (here $\gamma_{z'}$) and γ_s (here $\gamma_{x'}$ and $\gamma_{y'}$) respectively.

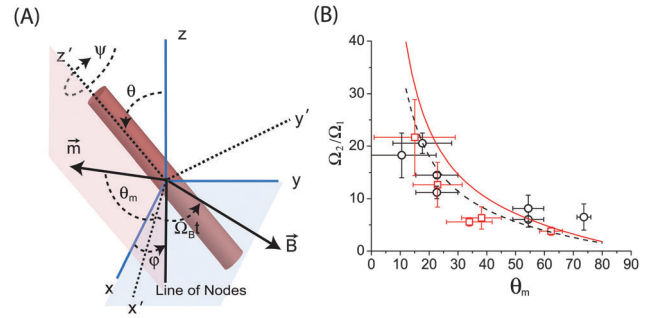

Fig. 2 (A) The Euler angles ϕ, θ and ψ used to define the instantaneous orientations of a nanorod, having a permanent moment m, under a magnetic field B, rotating at a frequency Ω_B. The direction of the moment is at angle θ_m to the short axis of the rod. (B) Experimentally obtained ratio $\frac{\Omega_2}{\Omega_1}$ for different nanostructures. Red (solid) and black (dotted) lines show the theoretically obtained ratio of the two frequencies for two different aspect ratio propellers 5.8 and 5, respectively. It may be noted that as the ratio of the two frequencies is calculated, no adjustable parameter (like magnetic moment) is required to obtain the theoretical curve. Red squares and black circles are the corresponding experimental ratios for the two aspect ratios respectively, with error bars shown for both the measured values of θ_m and $\frac{\Omega_2}{\Omega_1}$. Black circles are the experimental values taken from ref. 24.

The magnetic field in the body frame ($x'y'z'$ frame) is given by

$$\begin{bmatrix} B_{x'} \\ B_{y'} \\ B_{z'} \end{bmatrix} = R \times \begin{bmatrix} B\cos(\Omega_B t) \\ B\sin(\Omega_B t) \\ 0 \end{bmatrix}, \quad (2)$$

where R is the transformation matrix and t represents the time elapsed.

Solving eqn (2), we get

$$B_{x'} = B(\cos\beta\cos\psi + \sin\beta\cos\theta\sin\psi), \quad (3)$$

$$B_{y'} = B(\sin\beta\cos\theta\cos\psi - \cos\beta\sin\psi), \quad (4)$$

$$B_{z'} = -B\sin\beta\sin\theta, \quad (5)$$

where $\beta = \Omega_B t - \phi$.

Resolving the magnetic moment m, which is supposed to be in the body $x'z'$ plane, we get $m_{x'} = m\cos\theta_m$, $m_{y'} = 0$ and $m_{z'} = m\sin\theta_m$. So, the magnetic torque in the body frame is given by

$$\begin{bmatrix} \tau_{x'} \\ \tau_{y'} \\ \tau_{z'} \end{bmatrix} = \begin{vmatrix} \hat{i} & \hat{j} & \hat{k} \\ m\cos\theta_m & 0 & m\sin\theta_m \\ B_{x'} & B_{y'} & B_{z'} \end{vmatrix}. \quad (6)$$

Solving eqn (6), using eqn (3)–(5), we get

$$\tau_{x'} = mB\sin\theta_m(\cos\beta\sin\psi - \sin\beta\cos\theta\cos\psi), \quad (7)$$

$$\tau_{y'} = mB(\sin\theta_m\sin\beta\cos\theta\sin\psi + \sin\theta_m\cos\beta\cos\psi + \cos\theta_m\sin\beta\sin\theta), \quad (8)$$

$$\tau_{z'} = mB\cos\theta_m(\sin\beta\cos\theta\cos\psi - \cos\beta\sin\psi). \quad (9)$$

The body frame angular velocities are given by

$$\omega_{x'} = \dot{\phi}\sin\theta\sin\psi + \dot{\theta}\cos\psi, \quad (10)$$

$$\omega_{y'} = \dot{\phi}\sin\theta\cos\psi - \dot{\theta}\sin\psi, \quad (11)$$

$$\omega_{z'} = \dot{\phi}\cos\theta + \dot{\psi}. \quad (12)$$

Solving for $\dot{\phi}$, $\dot{\theta}$ and $\dot{\psi}$, from eqn (10)–(12) and using the Stokes equation, we get

$$\dot{\phi} = \frac{mB}{\gamma_s\sin\theta}(\sin\theta_m\cos\beta + \cos\theta_m\sin\beta\sin\theta\cos\psi), \quad (13)$$

$$\dot{\theta} = -\frac{mB}{\gamma_s}\sin\beta(\sin\theta_m\cos\theta + \cos\theta_m\sin\theta\sin\psi), \quad (14)$$

$$\dot{\psi} = \frac{mB\cos\theta_m(\sin\beta\cos\theta\cos\psi - \cos\beta\sin\psi)}{\gamma_l} - \dot{\phi}\cos\theta. \quad (15)$$

The steady state configuration of the object for a particular Ω_B can be defined as the orientation where the angles θ and ψ remain constant in time, given by,

$$\dot{\theta} = 0, \quad (16)$$

$$\dot{\psi} = 0. \quad (17)$$

A steady state configuration defined in this manner can be either in (a) a phase locked state (where the magnetic moment can follow the magnetic field, *i.e.* $\dot{\phi} = \Omega_B$) or (b) a phase slipped state (where the magnetic moment cannot follow the magnetic field, *i.e.* $\dot{\phi} \neq \Omega_B$).

The steady state eqn (16) can be valid under two possible conditions:

(i) $\theta = \frac{\pi}{2}$ and $\psi = 0$;

or

(ii) $\beta = n\pi$, where n is an integer.

Condition (i) automatically satisfies eqn (17) and is therefore a valid solution to eqn (1). Physically it refers to the tumbling condition, with the corresponding equation for $\dot{\phi}$ given by,

$$\dot{\phi} = \frac{mB}{\gamma_s}\sin(\theta_m + \beta). \quad (18)$$

Solving the differential equation eqn (18), we get

$$\phi = \theta_m + \Omega_B t - 2\arctan\left[\frac{mB}{\gamma_s\Omega_B} + C_2\left(\frac{C_1 + \exp(C_2\Omega_B t)}{C_1 - \exp(C_2\Omega_B t)}\right)\right], \quad \text{if } \Omega_B \leq \frac{mB}{\gamma_s}, \quad (19)$$

$$= \theta_m + \Omega_B t - 2\arctan\left[C_3 + \sqrt{1 - C_3^2}\tan\left(\frac{\Omega_B t\sqrt{1 - C_3^2}}{2} - \arctan\left(\frac{C_3}{\sqrt{1 - C_3^2}}\right)\right)\right], \quad \text{if } \Omega_B > \frac{mB}{\gamma_s}, \quad (20)$$

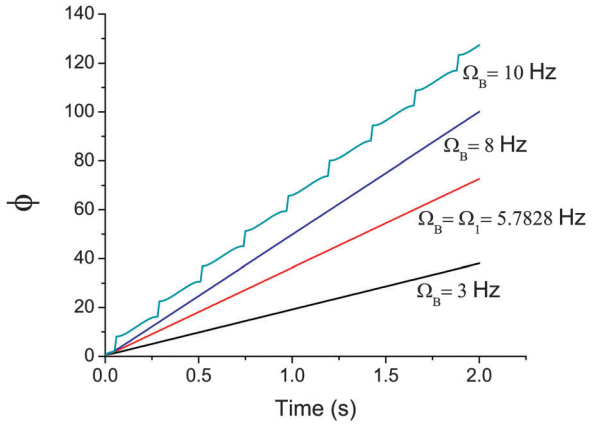

Fig. 3 Theoretical plot of ϕ *vs.* time at different frequencies for $\theta = 90^\circ$ (tumbling). It shows that after $mB/\gamma_s = 8.58$ Hz, ϕ becomes non linear in time.

where,

$$C_1 = \frac{\frac{mB}{\gamma_s \Omega_B} - C_2}{\frac{mB}{\gamma_s \Omega_B} + C_2},$$

$$C_2 = \sqrt{\left(\frac{mB}{\gamma_s \Omega_B}\right)^2 - 1},$$

$$C_3 = \frac{mB}{\gamma_s \Omega_B}$$

Fig. 3 shows the plot of ϕ *vs.* t for different Ω_B from which it is clear that the ellipsoid can tumble in a phase locked state while $\Omega_B \leq \frac{mB}{\gamma_s}$. This is reasonable for tumbling motion since till a frequency equal to $\frac{mB}{\gamma_s}$, the magnetic moment of the object can follow the applied magnetic field with a constant phase difference. Beyond this frequency, the angle between $\vec{m}$ and $\vec{B}$ becomes more than 90° with $\theta = 90^\circ$, thus causing phase slip. Note that we have not considered the stability of tumbling motion in this analysis, although we have shown that tumbling is a valid solution to eqn (1) at all frequencies, where $0 < \Omega_B \leq \frac{mB}{\gamma_s}$ and $\Omega_B > \frac{mB}{\gamma_s}$ imply phase locked and phase slipped tumbling respectively.

Using the second condition for steady state (*i.e.* $\beta = n\pi$) in eqn (13), we get

$$\dot{\phi} = \pm\frac{\omega_1}{\sin\theta}, \tag{21}$$

where $\omega_1 = \frac{mB\sin\theta_m}{\gamma_s}$ and the sign depends upon whether n is even or odd respectively. We neglect the unphysical solution of n being an odd integer, as it implies $\theta > \pi$. Finally, assuming the precession angular speed $\dot{\phi} = \Omega_B$ corresponding to phase locked state, we get

$$\Omega_B = \frac{\omega_1}{\sin\theta}. \tag{22}$$

We can also find the steady state value of ψ using the second condition for steady state (*i.e.* $\beta = n\pi$) and eqn (13), (15) and (17),

$$\sin\psi = \frac{-\Omega_B \gamma_l}{mB\cos\theta_m}\cos\theta. \tag{23}$$

From here, the steady state value of ψ is obtained as

$$\sin\psi = \mp\frac{\gamma_l\sqrt{\Omega_B{}^2 - \omega_1{}^2}}{mB\cos\theta_m}, \tag{24}$$

depending on the condition whether $\theta < 90^\circ$ and $\theta > 90^\circ$ respectively.

The analysis proves that the object can show precessional phase locked motion ($\theta \neq 90^\circ$) if and only if $\Omega_B > \omega_1$. We shall prove later with stability analysis that $\Omega_1 = \omega_1 = \frac{mB\sin\theta_m}{\gamma_s}$, physically corresponds to the critical frequency at which the object stops tumbling and starts to precess. The precessional phase locked motion continues till the frequency at which the angle between $\vec{m}$ and $\vec{B}$ reaches 90°. We refer to this critical frequency as Ω_2, beyond which the motion is phase slipped. Derivation for the expression of Ω_2 is as follows: let δ be the angle between m and B. So, we can write

$$m_{x'}B_{x'} + m_{z'}B_{z'} = mB\cos\delta. \tag{25}$$

Expanding eqn (25) and using $\sin\beta = 0$, we get

$$\cos\delta = \cos\theta_m\cos\psi. \tag{26}$$

As we know, the step out frequency Ω_2 is reached when $\delta = 90^\circ$. Considering this condition in eqn (26), at frequency Ω_2, the value of ψ becomes $\mp 90^\circ$, depending on the whether $0^\circ \leq \theta < 90^\circ$ or $90^\circ < \theta \leq 180^\circ$. Now, taking into consideration the steady state and phase locked conditions for precession, we get

$$-\frac{mB\cos\theta_m\sin\psi}{\gamma_l} = \Omega_B\cos\theta. \tag{27}$$

Considering $\psi = \mp 90^\circ$ and $\theta = \theta_2$ at $\Omega_B = \Omega_2$, eqn (27) can be written as

$$\Omega_2 = \pm\frac{mB\cos\theta_m}{\gamma_l\cos\theta_2}. \tag{28}$$

Using the fact that $\Omega_2 = \frac{\Omega_1}{\sin\theta_2}$ and $\sin^2\theta_2 + \cos^2\theta_2 = 1$, we get the required expression for Ω_2, which is

$$\Omega_2 = mB\sqrt{\left(\frac{\sin\theta_m}{\gamma_s}\right)^2 + \left(\frac{\cos\theta_m}{\gamma_l}\right)^2}. \tag{29}$$

To summarize, the analysis so far reveals that phase locked tumbling is possible if $0 < \Omega_B \leq \frac{mB}{\gamma_s}$, whereas phase locked

precession is possible if $\Omega_1 < \Omega_B \leq \Omega_2$. It is also proved that below Ω_1, precessional motion cannot occur. Phase slipped tumbling and phase slipped precession occur beyond mB/γ_s and Ω_2 respectively. Beyond Ω_2, both types of motion are phase slipped, and have not been considered in this paper.

It is important to consider the physical significance of the above analysis for two important limiting cases. For a rod with magnetic moment along the long axis, *i.e.* $\theta_m = 90^\circ$, we obtain $\Omega_1 = \frac{mB}{\gamma_s} = \Omega_2$, implying the motion (tumbling) of the rod to be in the plane of the rotating field across the frequency spectrum, which was the case with many[2,10,11] magnetically or electrically driven nanorods in previous experiments. On the other hand, for an elongated object with magnetic moment along the short axis, *i.e.* $\theta_m = 0^\circ$, $\Omega_1 = 0$, which include magnetically driven helical[17,18] nanostructures used for nanoscale propulsion, we get $\Omega_2 = \frac{mB}{\gamma_l}$, implying motion around the long axis with $\theta = 0^\circ$ at all frequencies.

Fig. 2B plots the experimentally observed ratio $\frac{\Omega_2}{\Omega_1}$ against the measured values of θ_m for two helical nanostructures with slightly different aspect ratios of 5 and 5.8. The lines shown correspond to the theoretical estimates obtained using the formulae given before. As seen from the figure, the theoretical graphs approximately follow the trend of the experimental data within experimental errors. Note that interactions with the surface or other rods in close proximity could affect the experimental results, which have not been considered in the theoretical analysis.

IV Stability analysis

Fig. 4 shows a summary of the analytical solutions and their stability against small perturbations. Mathematically it has already been proven that the object can tumble at all rotational frequencies, while it can precess at all frequencies above Ω_1. These dynamical states can be either phase locked or phase slipped, depending on the frequency and whether it is tumbling or precessing. The numerical analysis is done by considering the time series of the angle θ, obtained through numerical solutions of the equations eqn (13)–(15) (details in the ESI,† S2). In the frequency range $\Omega_B < \Omega_1$, only tumbling can occur. Numerically, this was confirmed by various initial conditions of θ ($t = 0$), in all of which the steady state configuration was obtained to be tumbling, *i.e.* $\theta = \pi/2$. The stability was analyzed by adding a small instantaneous perturbation of magnitude 0.1° at some arbitrary instant to the time series and watching the temporal evolution of the precession angle (see Fig. S2A of the ESI†). After a short transient, the motion was found to return to the steady tumbling state, thereby proving that the dynamical state was indeed stable. A dramatically different behavior was observed in the frequency range $\Omega_1 < \Omega_B \leq \frac{mB}{\gamma_s}$, where both tumbling and precessional motion were valid solutions to the equations, but only the precessional motion was found to be stable against small perturbations. This confirms our previous ansatz that $\Omega_1 = \frac{mB\sin\theta_m}{\gamma_s}$ indeed corresponds to the experimental frequency Ω_1^{expt} at which the objects came out of the plane of the rotating field (*i.e.* stopped tumbling) and started to precess.

In the frequency region between mB/γ_s and Ω_2, the existence of another time scale could be observed, denoted by the frequency Ω_s, around which the dependence on the initial conditions and the effects of small numerical perturbations made important differences to the evolution of the time series. While we do not have a clear analytical understanding of the origin of Ω_s, it was found to be $\approx 0.7\ \Omega_2$, as obtained through numerical calculations (discussed below). Stability analysis revealed tumbling motion to be unstable (see Fig. S2B of the ESI†), while precessional motion was found to be stable (see Fig. S2C of the ESI†) against small perturbations in the frequency region $\Omega_1 < \Omega_B < \Omega_s$.

In the frequency region $\Omega_s \leq \Omega_B \leq \Omega_2$, the evolution of the time series was found to be strongly dependent on the initial conditions. The final state corresponded to either tumbling or precessional motion, and both were stable against small perturbations (see Fig. S2D in the ESI†). To investigate this point further, we analyzed our time series for 200 randomly chosen initial conditions of θ between 0° and 90°, such as to count the number of initial conditions (N_T) that finally evolved to a stable tumbling configuration. The probability (N_T/N) of occurrence of stable tumbling as a function of the magnetic field frequency (Ω_B), scaled by Ω_2, for different values of the magnetization angle θ_m, is shown in Fig. 5. As expected, in the low frequency regime, the object always showed phase locked tumbling such that $N_T/N = 1$. As the frequency went above Ω_1, the dynamics changed from stable tumbling to stable precession, making $N_T/N = 0$. At frequencies above Ω_s ($\approx 0.7\ \Omega_2$), for certain initial conditions, stable tumbling configurations were observed, implying $0 < N_T/N < 1$. The relation Ω_s ($\approx 0.7\ \Omega_2$) was found to be valid for all magnetization angles (θ_m) considered, except for $\theta_m = 90^\circ$, for which we get $N_T/N = 1$ at all $\Omega_B < \Omega_2$.

The existence of the frequency Ω_s beyond which it is possible to have stable precessional and tumbling motion is perhaps related to the recently observed bistable behavior in a related system,[24,26] where helical nanostructures were observed to switch randomly between tumbling and precession around Ω_2.

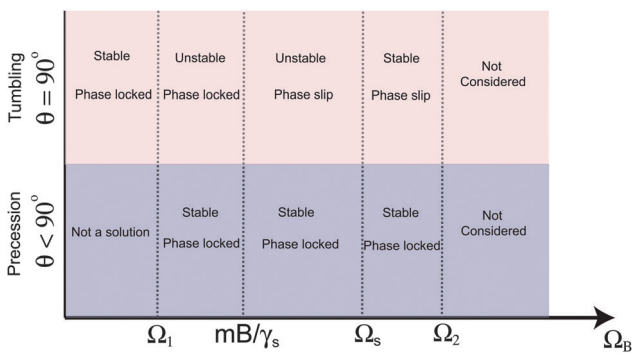

Fig. 4 Summary of the solutions for the dynamical configurations and their stabilities as a function of frequency.

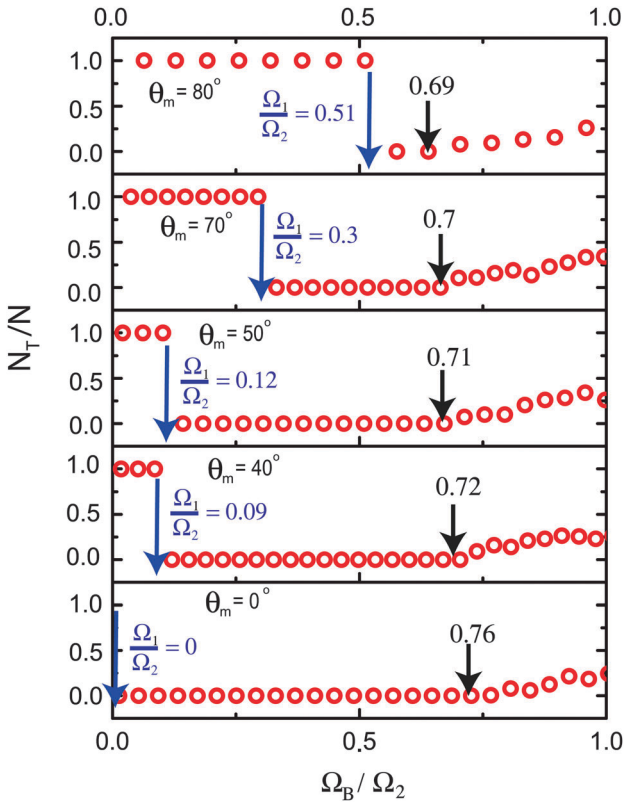

Fig. 5 Numerical data showing the probability to reach a stable tumbling state for different values of θ_m as a function of the frequency of the magnetic field.

The numerical analysis reported here did not take into account the effect of thermal noise, which could have important effects in the exact value of Ω_s. Preliminary results (see ESI,† S3) from the simulations show a rise in the value of Ω_s, when thermal noise is included in the numerical analysis.

V Conclusion

While an analytical theory of the rotational dynamics of an isolated sphere under an external torque is completely understood, the same is not true for the rotation of an isolated elongated object in systems dominated by viscous forces. The general approach towards understanding the motion of non-spherical nanoscale objects, including a wide class of macromolecules,[27] has been through numerical[25,28] calculations, which are necessary due to the complexity of the problem brought about by hydrodynamic interactions with other particles or the boundaries. However, even the case of an isolated non-spherical object under external torque has not been analytically solved, except for certain special cases where the external torque has specific directionality with respect to the body axis of the rod. The solution to the most general case has been achieved in this paper, where we have considered an isolated rod-like object having two different rotational drag coefficients and have shown that there can be different frequency dependent dynamical states. The theoretical analysis can be particularly useful in experiments where nanorods have been used for microrheological measurements, such as those based on magnetic rotational spectroscopy,[9] and could also aid in designing nanostructures of helical[17,18,29] and other[30] shapes used for nanoscale propulsion. The prediction from the stability analysis points towards a critical time scale, faster than which allows more than one dynamical state to be stable. The generality of this analysis is not limited to rods, but to any nanostructure whose rotational dynamics can be modeled with two drag coefficients.

Acknowledgements

The authors thank the Department of Biotechnology (DBT) and the Aeronautical Development Agency (ADA-NPMASS) for funding this work, and gratefully acknowledge the usage of the facilities in the Advanced Facility for Microscopy and Microanalysis (AFMM) and Micro and Nano Characterization Facility (MNCF, CeNSE) at IISc. This work is partially supported by the Ministry of Communication and Information Technology under a grant for the Centre of Excellence in Nanoelectronics, Phase II.

References

1 G. A. Ozin, I. Manners, S. Fournier-Bidoz and A. Arsenault, Dream nanomachines, *Adv. Mater.*, 2005, **17**(24), 3011–3018.
2 D. L. Fan, F. Q. Zhu, R. C. Cammarata and C. L. Chien, Controllable high-speed rotation of nanowires, *Phys. Rev. Lett.*, 2005, **94**(24), 247208.
3 A. D. Shine and R. C. Armstrong, The rotation of a suspended axisymmetric ellipsoid in a magnetic field, *Rheol. Acta*, 1987, **26**(2), 152–161.
4 P. Tierno, J. Claret, F. Sagués and A. Cēbers, Overdamped dynamics of paramagnetic ellipsoids in a precessing magnetic field, *Phys. Rev. E: Stat., Nonlinear, Soft Matter Phys.*, 2009, **79**(2), 021501.
5 W. Xi, A. A. Solovev, A. N. Ananth, D. H. Gracias, S. Sanchez and O. G. Schmidt, Rolled-up magnetic microdrillers: towards remotely controlled minimally invasive surgery, *Nanoscale*, 2013, **5**(4), 1294–1297.
6 M. Dienerowitz, M. Mazilu and K. Dholakia, Optical manipulation of nanoparticles: a review, *J. Nanophotonics*, 2008, **2**(1), 021875–021875.
7 M. Khan, A. K. Sood, F. L. Deepak and C. N. R. Rao, Nanorotors using asymmetric inorganic nanorods in an optical trap, *Nanotechnology*, 2006, **17**(11), S287.
8 W. A. Shelton, K. D. Bonin and T. G. Walker, Nonlinear motion of optically torqued nanorods, *Phys. Rev. E: Stat., Nonlinear, Soft Matter Phys.*, 2005, **71**(3), 036204.
9 A. Tokarev, I. Luzinov, J. R. Owens and K. G. Kornev, Magnetic rotational spectroscopy with nanorods to probe time-dependent rheology of microdroplets, *Langmuir*, 2012, **28**(26), 10064–10071.
10 N. Cappallo, C. Lapointe, D. H. Reich and R. L. Leheny, Nonlinear microrheology of wormlike micelle solutions using ferromagnetic nanowire probes, *Phys. Rev. E: Stat., Nonlinear, Soft Matter Phys.*, 2007, **76**(3), 031505.

11 L. Sun, K. Keshoju and H. Xing, Magnetic field mediated nanowire alignment in liquids for nanocomposite synthesis, *Nanotechnology*, 2008, **19**(40), 405603.
12 P. Bender, A. Günther, A. Tschöpe and R. Birringer, Synthesis and characterization of uniaxial ferrogels with ni nanorods as magnetic phase, *J. Magn. Magn. Mater.*, 2011, **323**(15), 2055–2063.
13 L. H. Lu, K. S. Ryu and C. Liu, A magnetic microstirrer and array for microfluidic mixing, *J. Microelectromech. Syst.*, 2002, **11**(5), 462–469.
14 P. Fischer and A. Ghosh, Magnetically actuated propulsion at low reynolds numbers: towards nanoscale control, *Nanoscale*, 2011, **3**(2), 557–563.
15 S. J. Ebbens and J. R. Howse, In pursuit of propulsion at the nanoscale, *Soft Matter*, 2010, **6**(4), 726–738.
16 J. J. Abbott, K. E. Peyer, M. C. Lagomarsino, L. Zhang, L. Dong, I. K. Kaliakatsos and B. J. Nelson, How should microrobots swim?, *Int. J. Rob. Res.*, 2009, **28**(11–12), 1434–1447.
17 L. Zhang, J. J. Abbott, L. Dong, B. E. Kratochvil, D. Bell and B. J. Nelson, Artificial bacterial flagella: fabrication and magnetic control, *Appl. Phys. Lett.*, 2009, **94**(6), 064107.
18 A. Ghosh and P. Fischer, Controlled propulsion of artificial magnetic nanostructured propellers, *Nano Lett.*, 2009, **9**(6), 2243–2245.
19 L. Zhang, T. Petit, Y. Lu, B. E. Kratochvil, K. E. Peyer, R. Pei, J. Lou and B. J. Nelson, Controlled propulsion and cargo transport of rotating nickel nanowires near a patterned solid surface, *ACS Nano*, 2010, **4**(10), 6228–6234.
20 B. A. Finlayson, Existence of variational principles for the navier-stokes equation, *Phys. Fluids*, 1972, **15**(6), 963–967.
21 J. R. Happel and H. Brenner, *Low Reynolds number hydrodynamics: with special applications to particulate media*, Springer, 1965, vol. 1.
22 A. Ortega and J. G. de la Torre, Hydrodynamic properties of rodlike and disklike particles in dilute solution, *J. Chem. Phys.*, 2003, **119**, 9914.
23 K. Keshoju, H. Xing and L. Sun, Magnetic field driven nanowire rotation in suspension, *Appl. Phys. Lett.*, 2007, **91**(12), 123114.
24 A. Ghosh, D. Paria, H. J. Singh, P. L. Venugopalan and A. Ghosh, Dynamical configurations and bistability of helical nanostructures under external torque, *Phys. Rev. E: Stat., Nonlinear, Soft Matter Phys.*, 2012, **86**(3), 031401.
25 K. E. Peyer, L. Zhang, B. E. Kratochvil and B. J. Nelson, Non-ideal swimming of artificial bacterial flagella near a surface. in *Robotics and Automation (ICRA), 2010 IEEE International Conference on*, IEEE, 2010, pp. 96–101.
26 V. M. Fomin, E. J. Smith, D. Makarov, S. Sanchez and O. G. Schmidt, Dynamics of radial-magnetized microhelix coils, *Phys. Rev. B: Condens. Matter Mater. Phys.*, 2011, **84**(17), 174303.
27 J. G. Kirkwood, *Recl. Trav. Chim. Pays-Bas*, 1949, **68**, 649; J. G. Kirkwood, *J. Polym. Sci.*, 1954, **12**, 1.
28 R. Kutteh, Rigid body dynamics approach to stokesian dynamics simulations of nonspherical particles, *J. Chem. Phys.*, 2010, **132**, 174107.
29 S. Tottori, L. Zhang, F. Qiu, K. K. Krawczyk, A. Franco-Obregón and B. J. Nelson, Magnetic helical micromachines: fabrication, controlled swimming, and cargo transport, *Adv. Mater.*, 2012, **24**(6), 811–816.
30 O. S. Pak, W. Gao, J. Wang and E. Lauga, High-speed propulsion of flexible nanowire motors: Theory and experiments, *Soft Matter*, 2011, **7**(18), 8169–8181.